



Finite-difference time-domain modeling of infrasound from pulsating auroras and comparison with recent observations

Sebastien de Larquier,¹ Victor P. Pasko,¹ Hans C. Stenbaek-Nielsen,² Charles R. Wilson,² and John V. Olson²

Received 10 December 2009; revised 28 January 2010; accepted 3 February 2010; published 23 March 2010.

[1] A FDTD model of infrasound propagation in a realistic atmosphere is used to provide quantitative interpretation of the recently reported infrasound signatures from pulsating aurora. The pressure perturbations observed on the ground are analyzed as a function of energy flux of precipitating auroral electrons and geometry and altitude localization of the source. The results indicate that fluxes on the order of 50 erg/cm²/s are needed to explain pressure wave magnitudes of 0.05 Pa observed on the ground. This energy is unlikely to be provided exclusively by precipitating electrons, and Joule heating associated with the electrojet modulated by the pulsating aurora may be responsible for part of the deposited energy. **Citation:** de Larquier, S., V. P. Pasko, H. C. Stenbaek-Nielsen, C. R. Wilson, and J. V. Olson (2010), Finite-difference time-domain modeling of infrasound from pulsating auroras and comparison with recent observations, *Geophys. Res. Lett.*, 37, L06804, doi:10.1029/2009GL042124.

1. Introduction

[2] Atmospheric infrasonic waves are acoustic waves with frequencies ranging from 0.02 to 10 Hz [e.g., *Blanc*, 1985]. Atmospheric infrasound is generated by a variety of sources, including volcanoes, tornadoes, earthquakes [e.g., *Bedard and Georges*, 2000], lightning [e.g., *Assink et al.*, 2008; *Pasko*, 2009], and sprites in the middle atmosphere [e.g., *Farges*, 2009]. The importance of infrasound studies has been emphasized in the past ten years from the Comprehensive Nuclear Test Ban Treaty (CTBT) verification perspective [e.g., *Le Pichon et al.*, 2009]. Infrasonic signals carry important information about their sources and correct modeling interpretation of observations therefore represents an important task for better understanding of dynamical features and energetics of infrasonic wave sources.

[3] Recently, *Wilson et al.* [2005] reported infrasonic signatures attributed to pulsating auroras observed by the infrasonic array I53US in Fairbanks, Alaska. Pulsating auroras are reported to have horizontal extents of 10 to 200 km [*Jones et al.*, 2009], vertical extents of 2 to 25 km [*Jones et al.*, 2009; *Stenbaek-Nielsen and Hallinan*, 1979; *Hallinan et al.*, 1985], and a pulse repetition period ranging from 1 to 40 s [*Johnstone*, 1978]. Infrasound signatures from pulsating auroras are attributed to the precipitation energetic flux particles into the upper atmosphere [e.g.,

Maeda and Watanabe, 1964; *Wilson et al.*, 2005; *Johnstone*, 1978]. The precipitation of energy is estimated using spectroscopic data from pulsating auroras and typically ranges from a few erg cm⁻² s⁻¹ (1 erg cm⁻² s⁻¹ = 10⁻³ J m⁻² s⁻¹) for weak pulsating auroras to 10–20 erg cm⁻² s⁻¹ for more energetic auroras, with a maximum of 25 erg cm⁻² s⁻¹ [*Davidson and Sears*, 1980].

[4] Although the morphology of pulsating auroral forms is well documented, the exact physical mechanisms of pulsating aurora still remain a subject of active debate [*Jones et al.*, 2009, and references therein]. The frequency domain coherence between the luminous intensity of the pulsating aurora and the infrasound received at the Earth surface have been investigated in [*Wilson et al.*, 2005; *Wilson and Olson*, 2005]. Video data of a pulsating aurora from an All-Sky video camera on the night of 5 December 2003 was compared with the pressure waveform data from the infrasonic array I53US at Fairbanks, Alaska. Enhanced coherence between the two signals was observed when a propagation delay time for the infrasound sample with respect to the video data sample was used. The required 5 to 6 minutes lag was consistent with the expected downward propagation time for waves from a source near 110 km altitude. The frequency domain coherence was found to be high between the pulsating aurora intensity above the array and the high trace-velocity infrasound signals at the surface in the pass band from 0.03 to 0.08 Hz. Ray-tracing studies indicate that such high trace-velocity infrasound signals originate from sources within 35 km of the zenith above the array for a source height of 110 km. The high coherence between the video and infrasound data lead authors to believe that periodic heating of the atmosphere by pulsating aurora is the source of the observed infrasound [*Wilson et al.*, 2005; *Wilson and Olson*, 2005].

[5] The specific task of the present paper is to undertake the first quantitative FDTD modeling of infrasound from pulsating aurora with particular emphasis on the source geometry and altitude.

2. Model Formulation

[6] The model employed in the present study utilizes linearized equations of acoustics with classical viscosity and atmospheric gravitational stratification effects to solve for perturbation in density, pressure and velocity [e.g., *Pasko*, 2009]. An attenuation term $-\xi\vec{v}$ is added to the momentum equation following an approach recently proposed by *de Groot-Hedlin* [2008].

[7] *Sutherland and Bass* [2004] provide a description of sound absorption in the atmosphere from the ground to 160 km altitude as a function of altitude and frequency. This

¹CSSL, Penn State University, University Park, Pennsylvania, USA.

²Geophysical Institute, University of Alaska, Fairbanks, Alaska, USA.

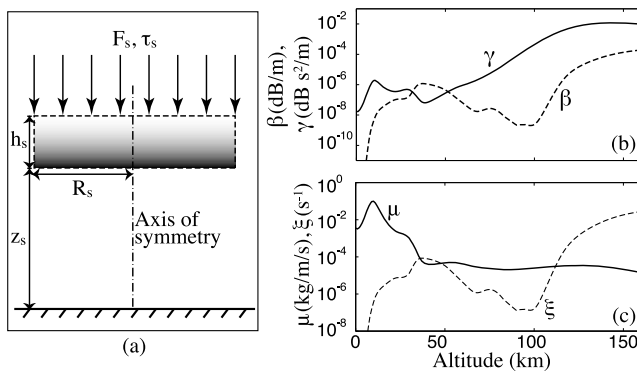


Figure 1. (a) Cross-sectional view of the model domain illustrating the parameters and geometry of the model. (b) Absorption coefficient β and γ as a function of altitude are computed for the frequency range 0.05–4 Hz and are in excellent agreement with Figure 1(a) of *de Groot-Hedlin* [2008]. (c) Coefficients μ and ξ .

frequency dependence makes it difficult to implement the absorption model in a FDTD model. *de Groot-Hedlin* [2008] proposed a decomposition technique based on a least-square fit of *Sutherland and Bass* [2004] attenuation coefficients by a quadratic function of frequency $\alpha(z, f) = \beta(z) + \gamma(z)f^2$. The same approach is used in our FDTD models, where the coefficients γ and β shown in Figure 1b are developed to match the terms describing absorption in the momentum conservation equation, including the viscosity term with viscosity coefficient $\mu = 3\rho_0 c_s^3 \gamma / 8\pi^2$ and additional attenuation term mentioned above with $\xi = 2c_s \beta$, where c_s is the ambient speed of sound and ρ_0 is the atmospheric ambient density. Figure 1c shows the altitude dependency of coefficients μ and ξ .

[8] The model equations are implemented in a one-dimensional (1-D) and a two-dimensional (2-D) axisym-

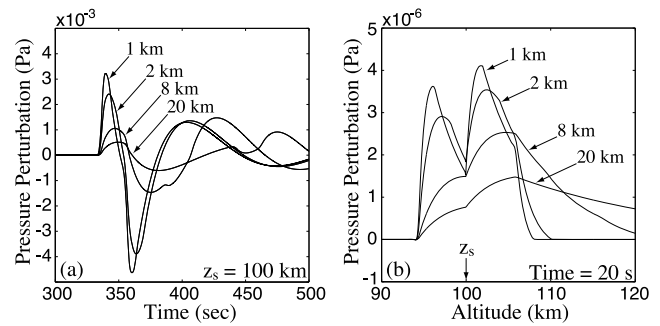


Figure 3. Comparison between model results obtained for different source vertical extents h_s . (a) Pressure perturbation observed on the ground for 4 different vertical extents of a source with $z_s = 100$ km. (b) Pressure perturbation at the end of the source excitation at time $t = \tau_s = 20$ s.

metric simulation domain using a second order in time and space FDTD scheme. An artificial viscosity [*Sparrow and Raspet*, 1991] is added to smooth the high frequency perturbations. A staggered grid as described by *Taflove and Hagness* [2000, pp. 75–79] is employed in space and time to respect the centering of the numerical method.

[9] The infrasonic source is modeled as a cylindrical layer of thickness h_s and radius R_s with lower boundary positioned at an altitude z_s as illustrated in Figure 1a. In the 1-D model, the cylindrical source converts into a slab of infinite horizontal extent. We assume that the precipitating particle energy flux F_s (in $\text{erg}/\text{cm}^2/\text{s}$ or $\text{J}/\text{m}^2/\text{s}$) is entirely converted into heat inside the cylinder during a given time τ_s . The distribution of that energy is assumed to decrease exponentially with height so that most of the energy is deposited toward the lower boundary of the source. The corresponding heat source can be expressed as $q(z, t) = (F_s/h_s) e^{-(z-z_s)/h_s}$ (in $\text{J}/\text{m}^3/\text{s}$) for $t \leq \tau_s$. The resulting pressure perturbation is derived from the first law of thermodynamics and included

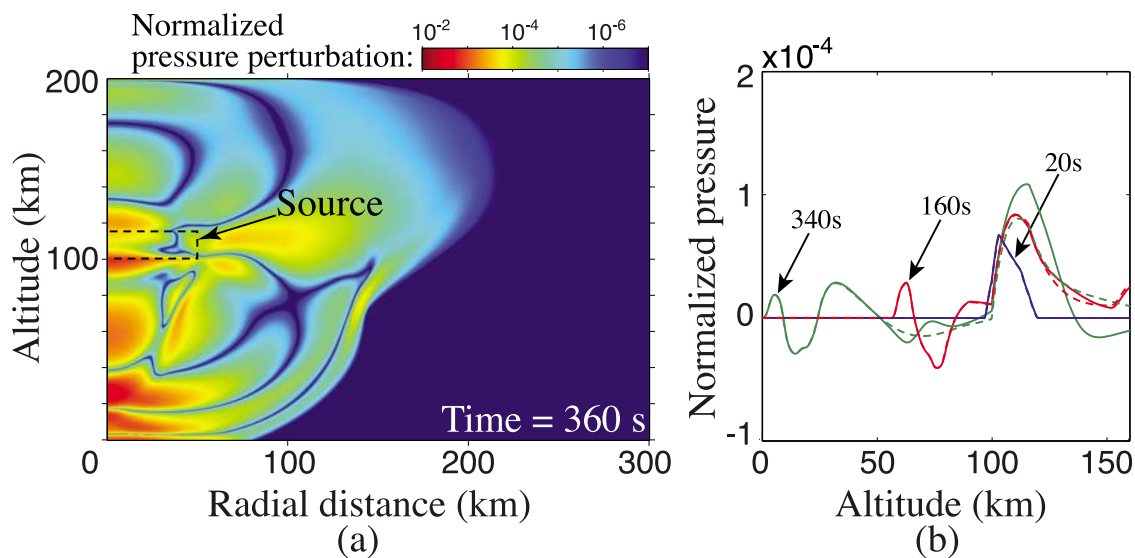


Figure 2. (a) Normalized magnitude of pressure perturbation obtained from the 2-D model for an $h_s = 8$ km thick source with $z_s = 100$ km observed at time 360 s. (b) Comparison between 1-D (solid lines) and 2-D (dashed lines) models at times 20, 120 and 340 s.

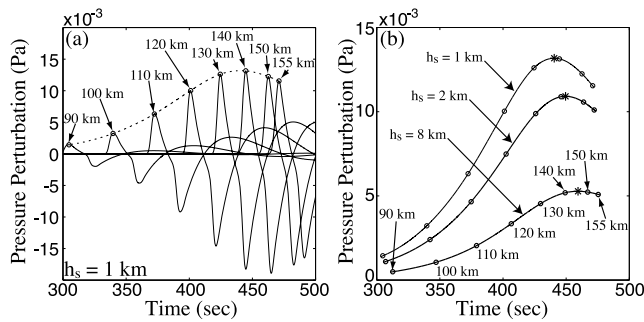


Figure 4. Comparison between model results obtained for a source positioned at different altitudes. (a) Pressure perturbation on the ground for a source vertical extent $h_s = 1$ km positioned at altitudes from 90 to 155 km. (b) The same analysis as in Figure 4a for sources with $h_s = 8, 2$ and 1 km.

in the energy conservation equation as $(\gamma' - 1)q$, where γ' is the ratio of specific heats [Maeda and Watanabe, 1964].

3. Results

[10] Both the 1-D and 2-D models are run using a value of the flux F_s of $5 \text{ erg/cm}^2/\text{s}$ as suggested by Johnstone [1978], and a heating time of $\tau_s = 20 \text{ s}$ as suggested by Royrvik and Davis [1977].

[11] The 2-D model is run for a source of vertical extent $h_s = 8 \text{ km}$ with its lower boundary at $z_s = 100 \text{ km}$ altitude and a radius $R_s = 50 \text{ km}$. Results in Figure 2 are presented in terms of normalized pressure perturbation $\tilde{p}/p_0(z) \sqrt{p_0(z)}/p_0(z_s)$. Figure 2a shows results from the 2-D model 360 seconds after initiation of the source. An observer on the ground placed anywhere from 0 to around 50 km from the axis would see a plane wave. Figure 2b compares the 2-D and 1-D model results at three instants in time, $t = 20, 160$ and 340 s . The pressure perturbation from the 2-D model is measured on the axis of the domain. There is a very good agreement between 1-D and 2-D models, thus suggesting that the use of the 1-D model is fully sufficient for this study, in agreement with similar conclusions reached by Wilson *et al.* [2005]. Unless mentioned otherwise, all results presented hereafter will be extracted from the 1-D model calculations.

[12] The influence of the source vertical extent on pressure perturbation observed on the ground is illustrated in Figure 3 for sources of vertical extent $h_s = 1, 2, 8$ and 20 km with a lower boundary set at $z_s = 100 \text{ km}$. Figure 3a evidences that the smaller the vertical extent, the higher the observed amplitude is. The same observation can be made from Figure 3b: after $t = \tau_s = 20 \text{ s}$, when all the energy has been deposited in the source volume, the pressure wave amplitude of the source with the smallest vertical extent is the highest.

[13] In Figure 4a, results for a source of vertical extent $h_s = 1 \text{ km}$ with its lower bound placed at $z_s = 90, 100, 110, 120, 130, 140, 150$ and 155 km altitude are presented. A similar analysis is conducted for sources with vertical extents $h_s = 2$ and 8 km . It appears that an increased source altitude leads to an increased observed pressure perturbation on the ground up to a given limit marked by a star on Figure 4b. Above that limit, the amplitude of the observed ground pressure

wave decreases when the altitude of the source lower boundary increases.

4. Discussion

[14] The 2-D model generates pressure perturbation that exhibits a plane wave structure when it reaches the ground, as evidenced by Figure 2a. The source radius $R_s = 50 \text{ km}$ chosen for the present study reasonably illustrates the wave structure created by a pulsating aurora. Jones *et al.* [2009, and references therein] report horizontal extents ranging from 10 to 200 km. The horizontal extent of the source relatively to its altitude explains the observed plane wave. Furthermore, the comparison of the pressure perturbation generated by the 1-D and 2-D models in Figure 2b shows a very good agreement between the two models. The agreement between 1-D and 2-D models is in full accord with observations by Wilson *et al.* [2005] of very high acoustic trace velocities that are characteristic of a plane wave coming from almost straight above the infrasonic array.

[15] The pressure perturbation created by the energy flux through the aurora layer should exhibit a $1/h_s$ dependency related to the assumption that a constant flux of energy is deposited into a variable volume: as the volume is reduced, the energy density has to increase to obtain the same total energy, hence the pressure perturbation amplitude increases [Maeda and Watanabe, 1964]. Results presented in Figure 3a do not, however, exactly reproduce the $1/h_s$ dependency. This difference is the manifestation of the speed of sound effects leading to propagation of the pressure wave outside of the heating volume during the heating time τ_s . At an altitude of $z_s = 100 \text{ km}$ the speed of sound is $c_s \simeq 290 \text{ m/s}$, so that for a source at that altitude after 20 s the pressure wave would have propagated almost 6 km. This means that for a source of vertical extent h_s larger than 6 km, we can consider that the energy is deposited almost instantaneously, and the $1/h_s$ dependency would be respected, whereas for a source smaller than 6 km, the pressure wave propagates outside of the source volume before all the energy has been deposited. Figure 3b shows that after 20 s, the break in the pressure perturbation curve, located at the lower vertical boundary of the source, is sharper for smaller sources, which indicates that more of the source pressure perturbation has propagated outside of the source volume.

[16] The pressure perturbation for the linear lossless propagation in a stratified atmosphere would scale as the square root of the ambient pressure $\tilde{p} \sim \sqrt{p_0}$ [Gossard and Hooke, 1975, p. 77; Maeda and Watanabe, 1964]. Figure 4a illustrates this effect as the observed ground amplitudes increase as the constant vertical extent source is placed at higher altitudes in the atmosphere. The amplification due to gravity stratification is, however, limited by absorption: the higher the source is initiated, the longer the path of the wave through the atmosphere will be. It can also be noticed from the expression of the absorption coefficient α given in section 2 that absorption is proportional to the square of frequency. Since larger sources can be characterized as having a larger wavelength and lower frequency, they will have a higher optimum initial height as shown in Figure 4b, simply reflecting stronger absorption of high frequency waves at higher altitudes in comparison with low frequency waves.

[17] Although a higher source altitude z_s gives us higher wave amplitudes on the ground, only sources between 90 and 110 km altitude fit the 5 to 6 min time lag between visual observation and infrasound measurements for the pulsating aurora observed by *Wilson et al.* [2005]. Pulsating auroras have been observed at altitudes higher than a 110 km [e.g., *Brown et al.*, 1976], but most observations suggest average altitudes between 90 and 110 km [e.g., *Stenbaek-Nielsen and Hallinan*, 1979].

[18] Modeling results presented in this work use heating rates equivalent to a precipitating electron flux $F_s = 5$ erg/cm²/s. For realistic source altitudes, 90 to 110 km, the resulting modeled pressure perturbations are roughly an order of magnitude smaller than those observed. Hence a source equivalent to a precipitating electron flux of 50 erg/cm²/s would be needed to obtain a pressure perturbation of 0.05 Pa on the ground. This is in agreement with previous estimates by *Maeda and Watanabe* [1964]. The energy flux of 5 erg/cm²/s may be too conservative. *Davidson and Sears* [1980] and *Sears and Vondrak* [1981] have reported values between 10 to 20 erg/cm²/s based on optical observations for more energetic pulsating auroras, with an observed maximum of 25 erg/cm²/s. We note that even this observed maximum produces a factor of two lower pressure perturbations than observed, suggesting possible additional sources. A possibility is Joule heating from ionospheric currents modulated by the pulsating aurora. *Weimer* [2005] and *Kosch and Nielsen* [1995] indicate that the energy input from Joule heating is of same order as the particle energy input while *Lu et al.* [1998] find Joule heating to be significantly more important. These studies were done on much larger spatial scales than the individual patches of pulsating auroras we are considering, and it is uncertain whether the same ratios apply here. Nevertheless, Joule heating is likely an important additional energy source, which needs further investigation.

[19] **Acknowledgments.** This research was supported by NSF ATM-0836391 to Penn State University and NSF ATM-0741641 to the University of Alaska Fairbanks.

References

- Assink, J. D., L. G. Evers, I. Holleman, and H. Paulssen (2008), Characterization of infrasound from lightning, *Geophys. Res. Lett.*, *35*, L15802, doi:10.1029/2008GL034193.
- Bedard, A. J., and T. M. Georges (2000), Atmospheric infrasound, *Phys. Today*, *53*(3), 32–37, doi:10.1063/1.883019.
- Blanc, E. (1985), Observations in the upper-atmosphere of infrasonic waves from natural or artificial sources—A summary, *Ann. Geophys.*, *3*(6), 673–687.
- Brown, N. B., T. N. Davis, T. J. Hallinan, and H. C. Stenbaek-Nielsen (1976), Altitude of pulsating aurora determined by a new instrumental technique, *Geophys. Res. Lett.*, *3*(7), 403–404, doi:10.1029/GL003i007p00403.
- Davidson, G. T., and R. D. Sears (1980), Pulsating aurorae—Evidence for flux limiting, *Geophys. Res. Lett.*, *7*(3), 185–188, doi:10.1029/GL007i003p00185.
- de Groot-Hedlin, C. (2008), Finite-difference time-domain synthesis of infrasound propagation through an absorbing atmosphere, *J. Acoust. Soc. Am.*, *124*(3), 1430–1441, doi:10.1121/1.2959736.
- Farges, T. (2009), Infrasound from lightning and sprites, in *Lightning: Principles, Instruments and Applications*, edited by H. D. Betz et al., 417–432 pp., Springer, New York.
- Gossard, E. E., and W. H. Hooke (1975), *Waves in the Atmosphere: Atmospheric Infrasound and Gravity Waves: Their Generation and Propagation*, 128 pp., Elsevier, Amsterdam.
- Hallinan, T. J., H. C. Stenbaek-Nielsen, and C. S. Deehr (1985), Enhanced aurora, *J. Geophys. Res.*, *90*(A9), 8461–8475, doi:10.1029/JA090iA09p08461.
- Johnstone, A. D. (1978), Pulsating aurora, *Nature*, *274*(5667), 119–126, doi:10.1038/274119a0.
- Jones, S. L., et al. (2009), PFISR and ROPA observations of pulsating aurora, *J. Atmos. Sol. Terr. Phys.*, *71*(6–7), 708–716, doi:10.1016/j.jastp.2008.10.004.
- Kosch, M. J., and E. Nielsen (1995), Coherent radar estimates of average high-latitude ionospheric Joule heating, *J. Geophys. Res.*, *100*(A7), 12,201–12,215, doi:10.1029/95JA00821.
- Le Pichon, A., J. Vergoz, E. Blanc, J. Guilbert, L. Ceranna, L. G. Evers, and N. Brachet (2009), Assessing the performance of the International Monitoring System's infrasound network: Geographical coverage and temporal variabilities, *J. Geophys. Res.*, *114*, D08112, doi:10.1029/2008JD010907.
- Lu, G., et al. (1998), Global energy deposition during the January 1997 magnetic cloud event, *J. Geophys. Res.*, *103*(A6), 11,685–11,694, doi:10.1029/98JA00897.
- Maeda, K., and T. Watanabe (1964), Pulsating aurorae and infrasonic waves in the polar atmosphere, *J. Atmos. Sci.*, *21*(1), 15–29, doi:10.1175/1520-0469(1964)021<0015:PAAIWI>2.0.CO;2.
- Pasko, V. P. (2009), Mechanism of lightning-associated infrasonic pulses from thunderclouds, *J. Geophys. Res.*, *114*, D08205, doi:10.1029/2008JD011145.
- Royrvik, O., and T. N. Davis (1977), Pulsating aurora: Local and global morphology, *J. Geophys. Res.*, *82*(29), 4720–4740, doi:10.1029/JA082i029p04720.
- Sears, R. D., and R. R. Vondrak (1981), Optical-emissions and ionization profiles during an intense pulsating aurora, *J. Geophys. Res.*, *86*(A8), 6853–6858, doi:10.1029/JA086iA08p06853.
- Sparrow, V. W., and R. Raspet (1991), A numerical-method for general finite-amplitude wave-propagation in 2 dimensions and its application to spark pulses, *J. Acoust. Soc. Am.*, *90*(5), 2683–2691, doi:10.1121/1.401863.
- Stenbaek-Nielsen, H. C., and T. J. Hallinan (1979), Pulsating auroras: Evidence for noncollisional thermalization of precipitating electrons, *J. Geophys. Res.*, *84*(A7), 3257–3271, doi:10.1029/JA084iA07p03257.
- Sutherland, L. C., and H. E. Bass (2004), Atmospheric absorption in the atmosphere up to 160 km, *J. Acoust. Soc. Am.*, *115*(3), 1012–1032, doi:10.1121/1.1631937.
- Taflove, A., and S. Hagness (2000), *Computational Electrodynamics: The Finite-Difference Time-Domain Method*, Artech, Boston, Mass.
- Weimer, D. R. (2005), Improved ionospheric electrodynamic models and application to calculating Joule heating rates, *J. Geophys. Res.*, *110*, A05306, doi:10.1029/2004JA010884.
- Wilson, C. R., and J. V. Olson (2005), Frequency domain coherence between high trace-velocity infrasonic signals at 153US and video data from pulsating aurora, *Inframatics*, *9*, 27–30.
- Wilson, C. R., J. V. Olson, and H. C. Stenbaek-Nielsen (2005), High trace-velocity infrasound from pulsating auroras at Fairbanks, Alaska, *Geophys. Res. Lett.*, *32*, L14810, doi:10.1029/2005GL023188.

S. de Larquier and V. P. Pasko, CSSL, Pennsylvania State University, 227 Electrical Engineering East, University Park, PA 16802, USA. (sdelarquier@psu.edu; vpasko@psu.edu)

J. V. Olson, H. C. Stenbaek-Nielsen, and C. R. Wilson, Geophysical Institute, University of Alaska, 903 Koyukuk Drive, Fairbanks, AK 99775, USA. (jvo@gi.alaska.edu; hnielsen@gi.alaska.edu; crw@gi.alaska.edu)